

Article

Secondary Recrystallization Goss Texture Development in a Binary Fe₈₁Ga₁₉ Sheet Induced by Inherent Grain Boundary Mobility

Zhenghua He ¹, Yuhui Sha ^{1,*}, Ning Shan ¹, Yongkuang Gao ¹, Fan Lei ¹, Fang Zhang ¹ and Liang Zuo ^{1,2}

¹ Key Laboratory for Anisotropy and Texture of Materials (Ministry of Education), Northeastern University, Shenyang 110819, China; hezhenghua@mail.neu.edu.cn (Z.H.); shanning_neu@126.com (N.S.); 18706304037@163.com (Y.G.); leifan1028@sina.com (F.L.); zhangf@smm.neu.edu.cn (F.Z.); lzuo@mail.neu.edu.cn (L.Z.)

² Institute of Metal Research, Chinese Academy of Sciences, Shenyang 110016, China

* Correspondence: yhsha@mail.neu.edu.cn; Tel.: +86-24-8369-1569

Received: 18 October 2019; Accepted: 20 November 2019; Published: 23 November 2019



Abstract: Secondary recrystallization Goss texture was efficiently achieved in rolled, binary Fe₈₁Ga₁₉ alloy sheets without the traditional dependence on inhibitors and the surface energy effect. The development of abnormal grain growth (AGG) of Goss grains was analyzed by quasi-situ electron backscatter diffraction (EBSD). The special primary recrystallization texture with strong {112}–{111}<110> and weak Goss texture provides the inherent pinning effect for normal grain growth by a large number of low angle grain boundaries (<15°) and very high angle grain boundaries (>45°) according to the calculation of misorientation angle distribution. The evolution of grain orientation and grain boundary characteristic indicates that the higher fraction of high energy grain boundaries (20–45°) around primary Goss grains supplies a relative advantage in grain boundary mobility from 950 °C to 1000 °C. The secondary recrystallization in binary Fe₈₁Ga₁₉ alloy is realized in terms of the controllable grain boundary mobility difference between Goss and matrix grains, coupled with the orientation and misorientation angle distribution of adjacent matrix grains.

Keywords: Fe-Ga alloy; secondary recrystallization; grain boundary character distribution; electron backscattered diffraction (EBSD); magnetostriction

1. Introduction

Giant magnetostrictive Fe-Ga alloy (Galfenol) is a promising magnetostrictive material for sensors and actuators applied in complex and harsh conditions due to the excellent combined magnetostrictive and mechanical properties [1–3]. The single crystals of Fe-Ga exhibit a magnetostriction coefficient up to –400 ppm along <100> crystallographic direction at the saturating fields (~200 Oe), which is lower than that for Terfenol-D (~2000 Oe) [2,3]. To break through the limit in applicability owing to the significant loss in metallic magnetic actuators caused by eddy current, a <100>-oriented Fe-Ga thin sheet with reduced eddy current loss in high-frequency actuated field is demanded [4,5]. Compared with slicing the highly textured Fe-Ga rods fabricated by the directional solidification process, Fe-Ga sheets with strong Goss texture ({110}<001>), through more efficient rolling and secondary recrystallization process, have attracted much attention recent years [6–9].

As with well-known grain-oriented silicon steel, secondary recrystallization of Goss-oriented grains requires three necessary conditions [10–12]: (1) normal grain growth of primary grains is effectively suppressed by precipitation particles called inhibitors so that fine-grained, primarily

recrystallized microstructure can provide enough driving force for abnormal growth; (2) some Goss grains have the priority of grain growth due to their special grain boundary characteristics [12–14]; (3) some Goss grains can break through the pinning and grow abnormally in favor of the grain boundary mobility advantage, and surface energy difference can also be used as the additional driving force [7,15]. Micron-sized particles of NbC are added in an Fe-Ga alloy sheet to suppress the growth of primary grains, and on this basis, the abnormal grain growth (AGG) of Goss grains is achieved by the surface energy effect from sulfur alloying or H₂S atmosphere. Na et al. [16,17] reported that nearly single-crystal Goss grains with magnetostriction coefficient of 300 ppm were developed in Fe₈₁Ga₁₉ sheets by combining 1–2.5 mol.% NbC micron particles with an H₂S + Ar atmosphere. Yuan and Liu et al. [18–20] obtained centimeters-sized Goss grains with a magnetostriction coefficient of 245 ppm at annealing atmosphere containing the sulfur element in Fe-Ga-based sheet added 0.1 mol.% NbC. Recently, magnetostriction coefficient of 285 ppm and secondary recrystallization Goss grains were induced by the dispersedly precipitated nanometer-sized sulfides and the well-matched pinning effect by the given primary recrystallization texture characteristic in Fe-Ga thin sheets [21].

When inhibitor and surface energy effects are applied to induce secondary recrystallization, it is critical to ensure the precise control of inhibitor distribution and surface composition in Fe-Ga alloy sheets. Moreover, the time-consuming purification annealing after complete secondary recrystallization is necessary to eliminate inhibitor constituents for the improvement of the magnetization performance. Consequently, if secondary recrystallization of accurate Goss grain is realized in binary Fe-Ga sheets, the complex and inefficient process, including inhibitor distribution and surface composition, as well as purification annealing, can be reduced. However, lower magnetostriction coefficients are obtained in binary Fe-Ga sheets due to less secondary recrystallization occurs without the necessary driving force [5,18,22]. Therefore, it is still a challenging problem to produce complete secondary recrystallization Goss texture in binary, thin, Fe-Ga sheets without using the inhibitor and the surface energy effect.

It is well known that high energy grain boundaries and coincidence site lattice (CSL) grain boundaries facilitate the AGG of Goss grains [10–14]. In previous research, we found that low angle grain boundaries play an important role in the formation of secondarily recrystallized Goss grains in binary Fe-Ga sheets [23]. However, the nucleation and growth of secondary recrystallization Goss texture and its relationship with grain boundary character distribution in a binary Fe-Ga alloy is still unclear. In this paper, special primary recrystallization texture morphology was prepared to introduce the difference in grain boundary mobility between Goss grains and matrix grains through regulating the grain boundary characteristic distribution, by which centimeter sized Goss grains, and large magnetostriction coefficients for binary Fe-Ga alloy were successfully achieved. The orientation and misorientation angle distribution during abnormal grain growth were analyzed by quasi-situ electron backscatter diffraction (EBSD) to clarify the formation mechanism of secondarily recrystallized Goss grain in binary Fe-Ga alloy sheet.

2. Materials and Methods

Fe₈₁Ga₁₉ alloy ingot was prepared by arc melting pure Fe (99.99%) and Ga (99.99%) elements under argon atmosphere. The 10 mm thick ingot was hot rolled at 1200 °C to 1.6 mm after two consecutive passes with a finishing temperature of 750 °C and then warm rolled under 200 °C to 0.55 mm with a reduction of 65%. The warm rolled sheets were first annealed at 750 °C for 10 min for primary recrystallization, and then heated from 750 °C to 1100 °C with a heating rate of 20 °C/h; next, quickly heated to 1200 °C and held for 60 min to complete secondary recrystallization under the flowing pure argon. Annealed samples were extracted at 800 °C, 900 °C, 950 °C, 975 °C, 1000 °C, and 1100 °C for characterizing the microstructure evolution. A detailed outline of the annealing process is shown in Figure 1a. The microstructure and grain orientation were observed by scanning electron microscope (SEM) (JEOL JSM 7001F, JEOL, Tokyo, Japan) with an EBSD acquisition system at an acceleration voltage of 15 kV and a working distance of 15 mm. Main texture components were calculated with a

deviation angle of 15° . The magnetostriction coefficients were calculated by $(3/2)\lambda_s = \lambda_{//} - \lambda_{\perp}$, where $\lambda_{//}$ and λ_{\perp} are the magnetostriction values measured by strain gauge method under the magnetic field from 0 to ± 150 kA/m applied parallel and perpendicular to the rolling direction, respectively.

To capture the nucleation and growth of secondarily recrystallized Goss grains, quasi-situ EBSD analysis on the interrupt annealed sample was conducted in a vacuum furnace from 950 to 1025 °C with a heating rate of 20 °C/h. The sample was taken out at temperature intervals of 25 °C and then rapidly cooled (20 °C/min) to analyze grain orientation and grain boundary character distribution (GBCD) by EBSD. The sample was reheated and annealed at the same heating rate after the EBSD acquisition. The vacuum degree was maintained higher than 2×10^{-4} Pa in the heating and cooling process to avoid deteriorating the quality of EBSD. The detailed outline for the interrupt annealing is shown in Figure 1b.

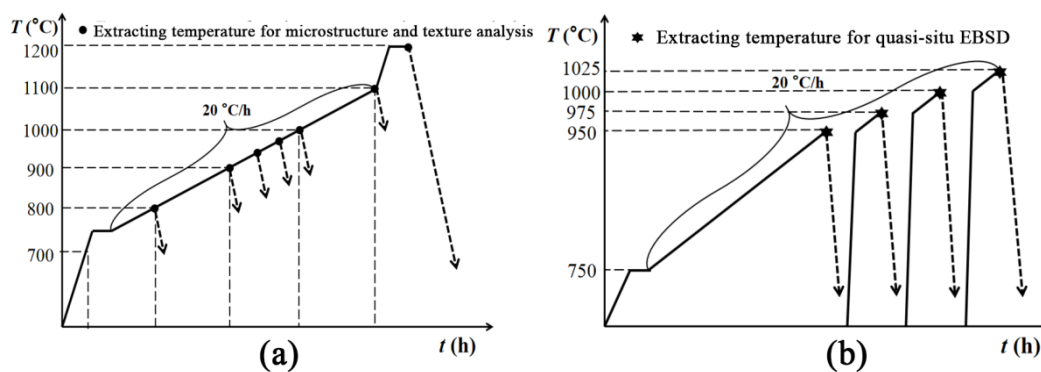


Figure 1. Flowchart of (a) annealing processes for microstructure and texture evolution, and (b) interrupted annealing for the quasi-situ electron backscatter diffraction (EBSD) analysis.

3. Results

3.1. Microstructure and Texture in Warm Rolled and Primarily Recrystallized Sheets

Figure 2 illustrates the microstructure and texture of warm rolled sheets. Shear bands are distributed widely at subsurface and in some are deformed grains of center layer. The shear bands in the quarter layer are shorter than in the center layer, which are closely related to the relatively coarse microstructure at center layer compared with quarter layer in hot bands [23]. Warm rolling texture consists mainly of α ($\langle 110 \rangle // RD$) and γ ($\langle 111 \rangle // ND$) fibers with peaks at $\{001\} \langle 110 \rangle$ and $\{111\} \langle 112 \rangle - \langle 110 \rangle$ respectively. The warm rolling microstructure and texture varying with the thickness layer lead to the difference in strain stored energy and nucleation sites, which inevitably affects the formation of recrystallization texture components.

Figure 3 presents the microstructure and texture of primarily recrystallized Fe-Ga sheets. The primary recrystallization microstructure features small grains ($\sim 23 \mu\text{m}$) in the subsurface layer and relatively large grains ($\sim 55 \mu\text{m}$) in the central layer. The overall primary recrystallization texture is composed of Goss γ and α components. While $\{112\} - \{111\} \langle 110 \rangle$ is the stronger texture at subsurface layer, $\{111\} \langle 112 \rangle$ and $\{113\} \langle 361 \rangle$ are the orientation density peaks at central layer. This primary recrystallization texture is different from the usual observation in grain-oriented silicon steels and Fe-Ga sheets, with strong $\{111\} \langle 112 \rangle$ and weak Goss at the subsurface layer [17–19,24,25].

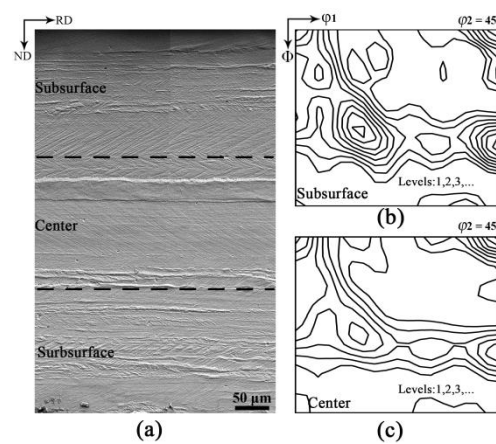


Figure 2. (a) Microstructure and constant $\varphi_2 = 45^\circ$ sections of orientation distribution functions (ODFs) (Levels: 1, 2, 3, ...) in (b) subsurface and (c) center layer of warm-rolled Fe-Ga sheets.

Accurate Goss grains nucleated at shear bands of $\{111\}\langle 112 \rangle$ deformed grains generally act as the sources of AGG Goss grains (Figure 3d) [26–28]. It was noted that Goss also was one of the main texture components in sheet thickness, which originated from widely distributed shear bands in γ deformed grains along the sheet thickness (Figures 2 and 3c) [29,30]. Stronger primarily recrystallized α and γ grains with smaller grain size develop preferentially at the subsurface layer due to more nucleation sites from relatively higher grain boundary areas and shorter shear bands in deformed grains.

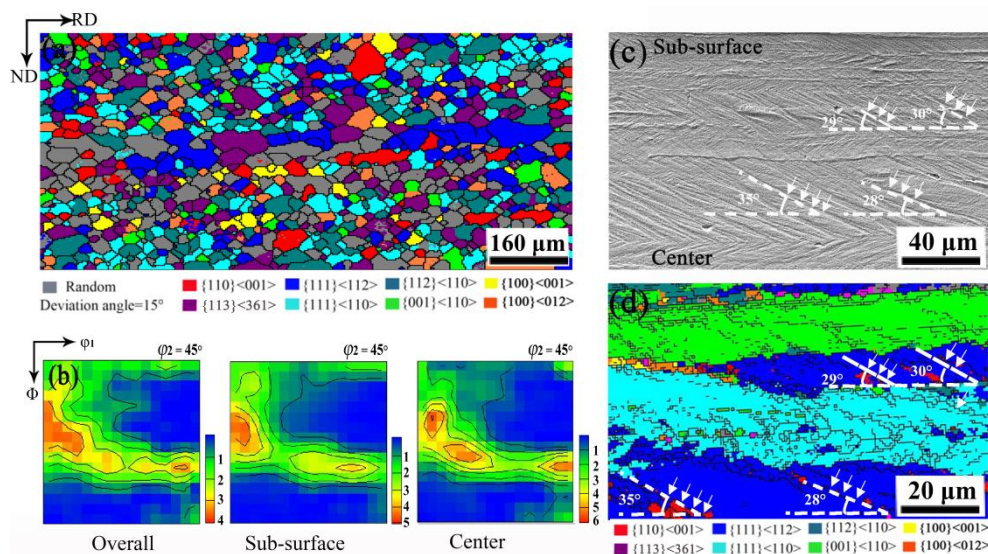


Figure 3. (a) Several main texture components, and (b) constant $\varphi_2 = 45^\circ$ sections of ODFs (Levels: 1, 2, 3, ...) of primarily recrystallized sheets (annealed at 750°C for 600 s). (c) Microstructure of warm-rolled sheets and (d) origin of Goss grains (in red) from shear bands in $\{111\}\langle 112 \rangle$ deformed grains (in blue) at a partially recrystallized state (annealed at 750°C for 20 s).

3.2. Microstructure, Texture, and Magnetostriction Evolution during the Heating Process

Figure 4 illustrates the microstructure and texture evolution during the heating process of $\text{Fe}_{81}\text{Ga}_{19}$ sheets. The fine grains in subsurface layer grow slightly to $25\ \mu\text{m}$ at 950°C , while the relatively coarse grains at center layer keep nearly stable at 1000°C . It was found that some abnormal grains occurred at subsurface layer as the annealing temperature exceeded 950°C , and the millimeter-sized grains accompanied by the matrix grains with the restricted average size of $65\ \mu\text{m}$ at 975°C . The abnormal grain growth began at the sub-surface layer, indicated by microstructure from the optical micrographs

(Figure 4c–e). Secondary recrystallization was nearly complete as the temperature rose to 1100 °C, featured by millimeters-sized grains throughout the sheet thickness.

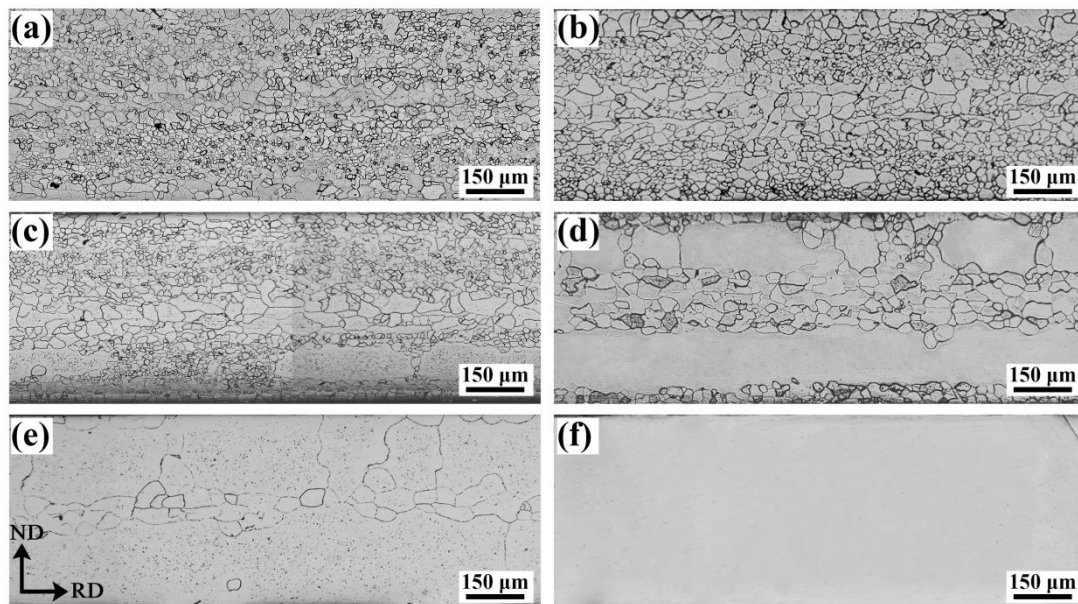


Figure 4. Microstructure evolution of $\text{Fe}_{81}\text{Ga}_{19}$ sheets at different heating temperatures: (a) 800 °C; (b) 900 °C; (c) 950 °C; (d) 975 °C; (e) 1000 °C; and (f) 1100 °C.

According to the microstructure in the rolling plane, secondary recrystallization first appears at 950 °C and completes at 1100 °C, while secondary grains grow rapidly around 975 °C and island grains substantially reduced at 1000 °C. The maximum grains have about 27 times larger grain size than matrix gains at 950 °C and further grow up to 35 times at 975 °C; the decrease of grain size ratio between maximum and matrix grains occurs at 1000 °C for the rapid grain growth of matrix grains (Figure 5). The main components of Goss, $\{111\}\langle 110 \rangle$ and $\{112\}\langle 110 \rangle$ are enhanced at the early stage of slow heating from 800 °C to 900 °C. It undergoes a major change at 950 °C—Goss texture is significantly enhanced (with orientation density of 25.3), while α and γ fibers are reduced. Goss texture is sharper with the rising temperature. The orientation density of Goss texture reaches up to 80.6 at 1100 °C, and further increases to 106.4 at 1200 °C with over 95% of the surface occupied by secondary Goss grains (Figure 6).

Figure 7 shows the magnetostriction coefficients of $\text{Fe}_{81}\text{Ga}_{19}$ sheets extracted from the furnace at different temperatures. It is noted that the occurrence of AGG Goss grains at 950 °C causes an evident increase in magnetostriction coefficient of 116 ± 19 ppm with respect to 65 ± 9 ppm at 900 °C where no AGG occurs [23]. Nearly complete secondary recrystallization with centimeter-sized Goss grain results in a larger magnetostriction coefficient of 233 ± 14 ppm at 1100 °C. The magnetostriction coefficient reaches up to 251 ppm after being annealed at 1200 °C due to the evident reduction of island grains. The magnetostriction coefficient obtained is larger than the previous reports about binary alloys [5,18,22], and close to the reported cases with both the inhibitors and the surface energy effect in Fe-Ga-based sheets [17,18]. It was noted that the parallel and perpendicular magnetostriction was not monotonously depended on the temperatures during the AGG of Goss grains. The slope of parallel magnetostriction for 950 °C is larger than that for 1000 °C. The saturation value of perpendicular magnetostriction for 1200 °C is even smaller than that for 1000 °C. It has been reported that the parallel and perpendicular magnetostriction are significantly related to the magnetic domain evolution during magnetization [31]. Therefore, the non-monotonous dependence of magnetostriction on temperature is mainly attributable to the change of magnetic domain, which is affected by the evolution of grain orientation and island grains during abnormal grain growth.

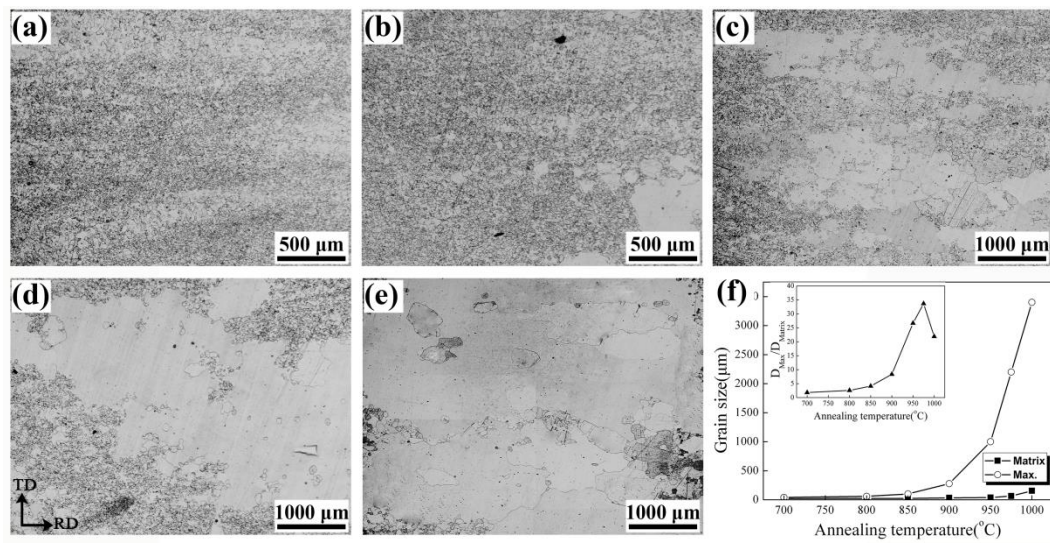


Figure 5. Microstructural evolution of Fe₈₁Ga₁₉ sheets at different heating temperatures: (a) 900 °C; (b) 950 °C; (c) 975 °C; (d) 1000 °C; and (e) 1100 °C; and (f) the grain size variations with temperature.

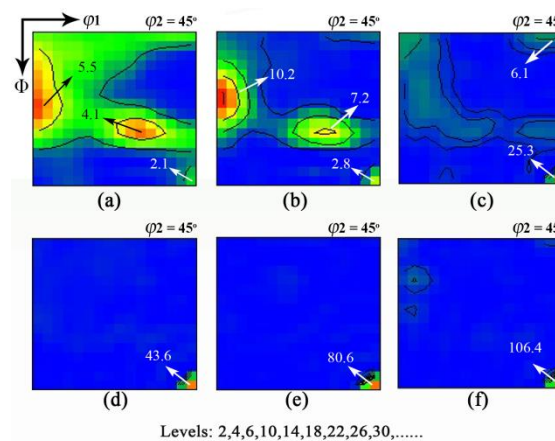


Figure 6. Constant $\varphi_2 = 45^\circ$ sections of ODFs of Fe₈₁Ga₁₉ sheets at different heating temperatures: (a) 800 °C; (b) 900 °C; (c) 950 °C; (d) 1000 °C; (e) 1100 °C; and (f) 1200 °C.

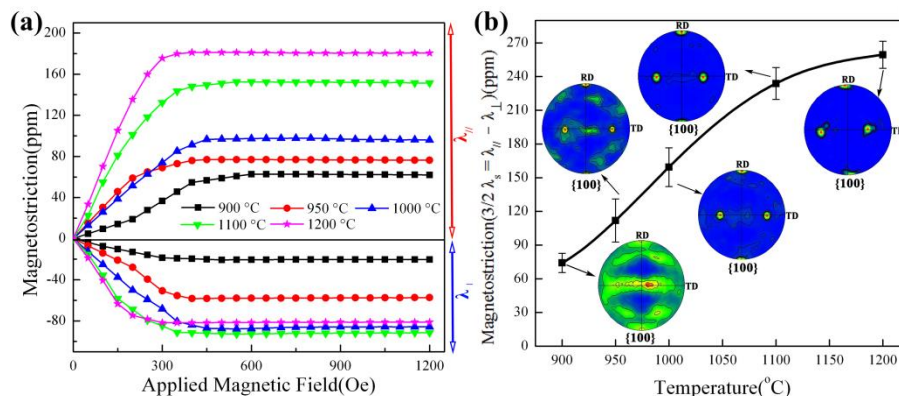


Figure 7. (a) Magnetostriction curves against with magnetic fields and (b) magnetostriction values against heating temperatures of the Fe₈₁Ga₁₉ sheets. Inset pole figures present the textures of the sheets.

3.3. The Nucleation and Growth of Secondary Recrystallization Using Quasi-Situ EBSD Measurement

The abnormal growth of Goss grains is usually considered to depend on the preferred grain boundary mobility when matrix grains are prohibited from growing by the pinning force of inhibitor.

However, there are no inhibitors as in the present study, so the critical question is how the preferred grain boundary mobility of Goss grains and the growth inhibition of matrix grains are realized to induce secondary recrystallization. It is known that the high energy grain boundary with medium misorientation angle ($\Delta\theta = 20\text{--}45^\circ$, HEGB) exhibits higher mobility than the low angle grain boundary ($\Delta\theta < 15^\circ$, LAGB) and high angle grain boundary ($\Delta\theta > 45^\circ$, HAGB) [32,33]. Therefore, the inherent difference in grain boundary mobility plays an important role in secondary recrystallization of Goss texture. The micro-textural evolution of annealing samples heated from 950 °C to 1025 °C was investigated by quasi-situ EBSD measurement to reveal the secondary recrystallization mechanism, as shown in Figure 8, and the inferred GBCDs are listed in Table 1.

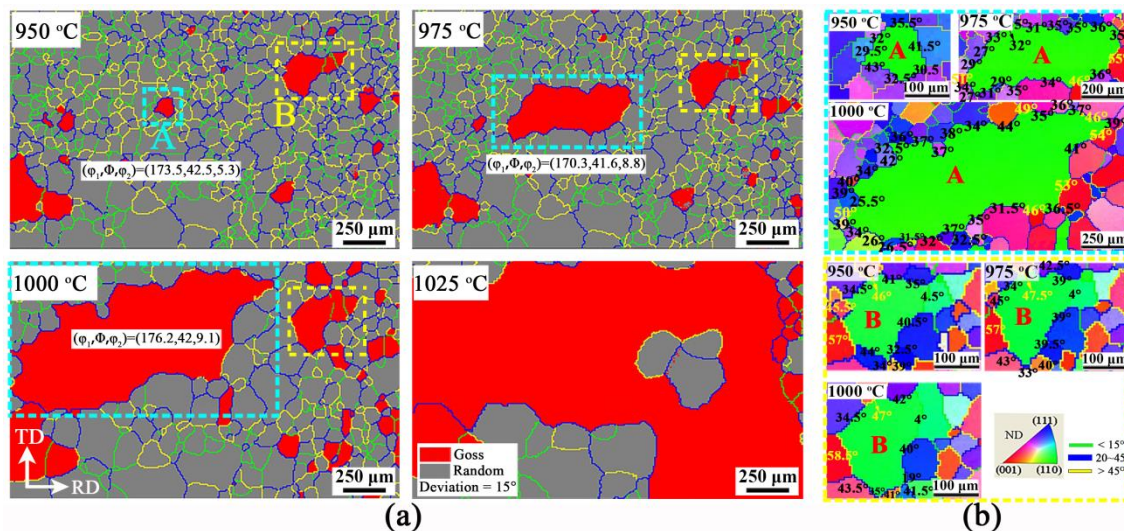


Figure 8. (a) Quasi-situ EBSD analysis and (b) local grain boundary characteristics of $\text{Fe}_{81}\text{Ga}_{19}$ sheets at annealing temperatures from 950 °C to 1025 °C.

Table 1. Grain boundary character distributions (GBCDs) of $\text{Fe}_{81}\text{Ga}_{19}$ sheets during heating from 950 °C to 1000 °C in Figure 4.

GBCD	950 °C (%)				975 °C (%)				1000 °C (%)			
	Matrix	Goss	A	B	Matrix	Goss	A	B	Matrix	Goss	A	B
<15°	22.6	6.0	0	8.1	20.9	6.2	1.2	6.1	17.6	8.7	2.1	12.6
20–45°	32.8	64.6	100	63.1	34.1	63.5	83.0	64.3	42.1	62.1	79.1	60.6
>45	34.1	25.1	0	27.5	35.2	26.2	14.5	28.0	33.8	25.4	16.8	20.4

It was found that a large number of LAGBs (green) and HAGBs (yellow) were distributed between adjacent matrix grains, and the total fraction of LAGB and HAGB of matrix grains was over 56% below 1000 °C. It is worthy of noting that both GBCDs and grain sizes of matrix grains are nearly stable below 1000 °C (Figure 8a), indicating that the matrix grains are effectively pinned. Abnormal growth grains derive from the matrix regions with more LAGBs and HAGBs and have a large fraction of HEGBs (blue). For instance, Goss grains A and B, indicated in Figure 8, are surrounded by more than 60% HEGBs from 975 °C to 1000 °C.

Actually, only a few Goss grains can grow abnormally, though most Goss grains have a higher fraction of HEGBs during heating according to the GBCD statistics in Table 1. This phenomenon was also reported in pure Fe-Si and Fe-Ga alloys [23,31,32]. Goss grain A, surrounded by more than 83% HEGBs below 1000 °C, rapidly annexes the matrix regions with more fine grains and low mobility grain boundaries, while Goss grain B, surrounded by lower than 65% HEGBs similar to other Goss grains, annexes partial small grains to normally grow up (Figure 8b) [33–35].

Figure 9 illustrates the grain orientation, deviation angle, and misorientation angle distribution of local regions of AGG grains in Fe₈₁Ga₁₉ sheets heated to 1000 °C and held for 20 min. The AGG Goss grains grow rapidly by annexing substantial matrix grains; and island grains at 1000 °C, within 20 min, relied on the advantages in grain size and grain boundary characteristics (Figure 9c). More non-HEGBs are formed around AGG Goss grains and the remaining matrix, which is partly attributable to the higher grain boundary mobility at this temperature. It was also found that the growth of AGG grains by consuming matrix grains lead to greater deviation for secondary recrystallization texture (Figure 9b) [36].

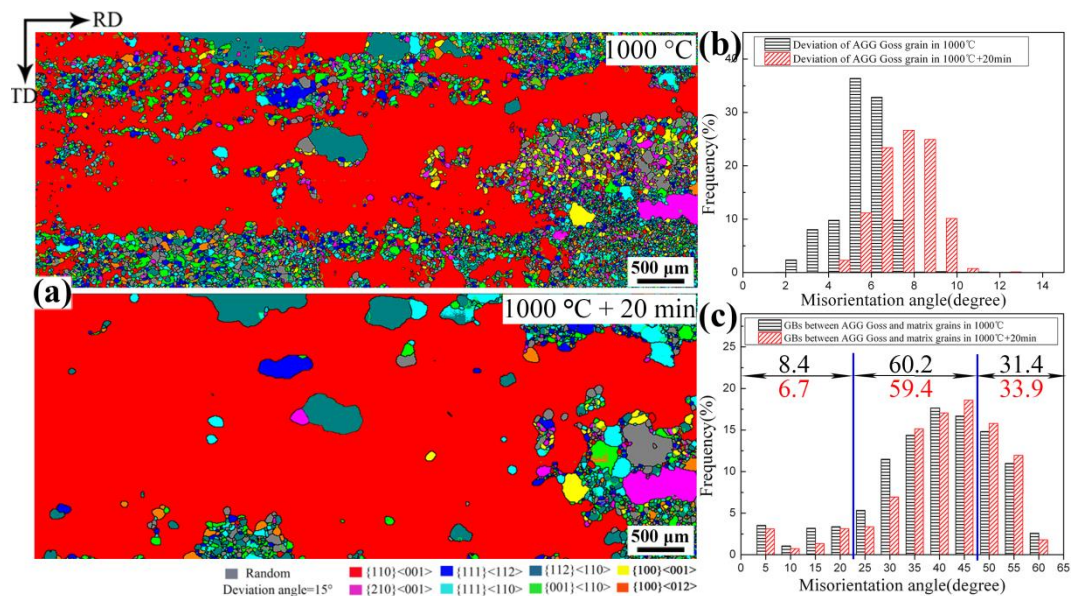


Figure 9. (a) Orientation image maps, (b) deviation angle, and (c) misorientation angle distributions of Goss grains in the quasi-situ EBSD of Fe₈₁Ga₁₉ sheets heated to 1000 °C and held for 20 min.

4. Discussion

4.1. Misorientation Angle Distribution at Primary Recrystallization

The key issue for secondary recrystallization is the preferred grain boundary mobility for Goss grains and the prohibition for the normal growth of matrix grains. Under the lack of additional pinning in binary Fe-Ga alloy, the driving force for secondary recrystallization mainly originates from the inherent grain boundary characteristic in primary recrystallization. It is known that the grain boundary energy and mobility are naturally related to its misorientation angle ($\Delta\theta$) [32,33], while HEGBs exhibit several times higher mobility than LAGBs and HAGBs.

The misorientation angle distribution is calculated based on the main texture components to represent the effects of primary recrystallization texture on grain boundary mobility [37]. Two orientation matrices are marked g_A and g_B , then the misorientation angle between A and B can be expressed as:

$$\Delta g_{AB} = g_A \cdot (g_B)^{-1} \quad (1)$$

Taking into account the 24 symmetries of cubic crystal system, the set of 1152 equivalent misorientation matrices is:

$$\Delta g_{AB}^k = \left\{ \begin{array}{c} O_i \cdot \Delta g_{AB} \cdot O_j \\ O_i \cdot (\Delta g_{AB})^{-1} \cdot O_j \end{array} \right\} (i, j = 1, 2, \dots, 24) \quad (2)$$

where O_i and O_j are the symmetric operating elements. The misorientation angle $\Delta\theta_k$ in each equivalent misorientation matrices satisfies:

$$\cos \Delta\theta_k = \left((\Delta g_{11}^k + \Delta g_{22}^k + \Delta g_{33}^k - 1) / 2 \right) (k = 1, 2, \dots, 1152) \quad (3)$$

The misorientation angle $\Delta\theta$ is obtained by taking the minimum value from 1152 equivalent misorientation angles $\Delta\theta_k$ from Equation (3):

$$\Delta\theta = \min \left\{ \cos^{-1} \left((\Delta g_{11}^k + \Delta g_{22}^k + \Delta g_{33}^k - 1) / 2 \right) \right\} (k = 1, 2, \dots, 1152) \quad (4)$$

The frequently observed texture components in body-centered cubic (BCC) alloy sheets are classified into three groups: α fiber ($\{001\}\langle 110\rangle$, $\{113\}\langle 110\rangle$, and $\{112\}\langle 110\rangle$), γ fiber ($\{111\}\langle 112\rangle$ and $\{111\}\langle 110\rangle$) and η fiber ($\{110\}\langle 001\rangle$, $\{210\}\langle 001\rangle$, and $\{100\}\langle 001\rangle$). Figure 10 illustrates the misorientation angle distribution of the main texture components on the constant $\varphi_2 = 45^\circ$ sections of Euler space. It can be seen that LAGBs mainly occur between $\{112\}\langle 110\rangle$ and $\{111\}\langle 110\rangle$, and HAGBs mainly occur between $\{001\}\langle 110\rangle$ and $\{111\}\langle 110\rangle$, and $\{001\}\langle 110\rangle$ and $\{111\}\langle 112\rangle$. Misorientation angles between Goss and most of the other texture components, including $\{111\}\langle 112\rangle$, $\{111\}\langle 110\rangle$, and $\{112\}\langle 110\rangle$, lie in the range of $20\text{--}45^\circ$.

Primary recrystallization texture in the present work, especially at subsurface layer, is composed of strong $\{112\}\langle 110\rangle$ and $\{111\}\langle 110\rangle$, weak $\{001\}\langle 110\rangle$, and Goss. A large number of LAGBs and HAGBs are formed in the matrix grains to stabilize the grain size during the heating process at a lower temperature until the approximate completeness of secondary recrystallization. The larger fraction of HEGBs around Goss grains can promote the preferred growth of Goss grains and further induces the AGG through sheet thickness with the help of the inhibited growth of matrix grains by LAGBs and HAGBs (Figure 8a). Therefore, the lower mobility of LAGBs and HAGBs can play a role in suppressing the growth of primary grains [23,33], and the mobility difference between HEGBs and low energy grain boundaries (LEGBs) acts as the driving force of secondary recrystallization in binary $\text{Fe}_{81}\text{Ga}_{19}$ alloy.

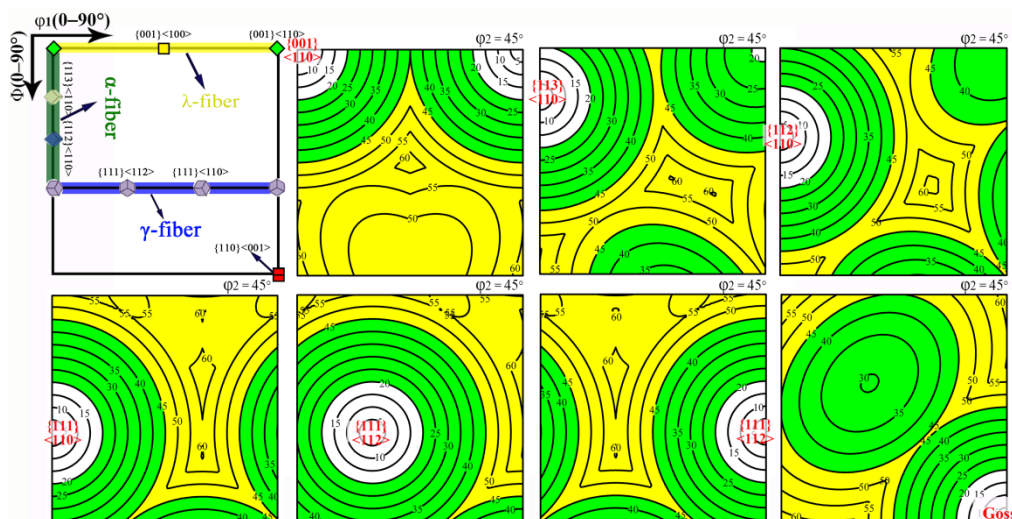


Figure 10. Misorientation angle distribution between the main texture components with red and the other texture components in constant $\varphi_2 = 45^\circ$ sections of Euler space.

4.2. Development of Secondary Recrystallization by Inherent Grain Boundary Mobility

An evident difference between Goss and matrix grains in grain boundary mobility is required for the secondary recrystallization of Goss grain. This difference is generally provided by the preferred coarsening of inhibitor around Goss grains or surface energy effects for (110) plane in Fe-Si and Fe-Ga alloys [12–17]. In binary Fe-Ga alloy, the preferred growth of Goss grain is significantly related to the

coherent difference in grain boundary mobility between HEGB and other grain boundaries [18,23]. It has been reported the high fraction of LAGBs in the matrix suppresses the grain growth below 1000 °C in Fe-Ga alloy [23]. In the present work, both the high fraction of LAGBs and HAGBs distributed between adjacent matrix grains provided inhibitor effectively to the normal grain growth below 1000 °C. The high fraction of HEGBs around Goss grains exhibits relatively higher mobility to promote the preferred grain growth. It was found the preferred growth of Goss grains derives from higher fraction of HEGBs ($\geq 60\%$) (Figure 8) and the abnormal Goss grain occurs with a much higher fraction of HEGBs ($\approx 80\%$) from 950 °C to 1000 °C.

However, the secondary recrystallization cannot occur in the local regions having high mobility of grain boundaries without the necessary driving force (Figure 8b) [11,34]. It can be inferred that besides the inherent grain boundary mobility advantage of Goss grains, the grain boundary characteristic and grain size of adjacent matrix grains also determine the amplitude of driving forces for AGG during the heating process. This is supported by the fact that Goss grain A preferentially annexes the left and upper matrix regions with more fine grains and low mobility grain boundaries, and rapidly develops into a secondary nucleus by virtue of the large fraction HEGBs ($\approx 80\%$) at the temperature range of 975–1000 °C, while Goss grain B annexes surrounded partial small grains to give priority to growth (Figure 8a). The abnormal Goss grains also preferentially annex the fine grains distributed to more low mobility grain boundaries [36], while the regions with more coarse grains and less low mobility grain boundaries are left to form island grains (located at the bottom right of Figure 9).

The annealing temperature range and heating rate must be also controlled to make full use of the coherent difference in grain boundary mobility for the AGG of Goss grains in binary Fe-Ga alloy [18,23]. At the temperature range of 950–1000 °C, Goss grains can grow rapidly by virtue of the large fraction of HEGBs (Figure 8), where the AGG of Goss grains generally appears in Fe-Ga alloy [18–21,23]. Abnormal Goss grains rapidly annex the matrix grains and island grains at the temperature of 1000–1025 °C (Figures 8a and 9a) [38]. A suitable heating rate can effectively maintain the difference in grain boundary mobility to ensure the development of secondary recrystallization [18–20].

In summary, the primary recrystallization texture morphology provides a coherent mobility difference between Goss grains and matrix grains by special misorientation angle distribution. The inherent mobility difference can be exploited for the suppression of primary grains and preferential growth of Goss grains under certain annealing temperature range and heating rate. The grain boundary characteristic and grain size of adjacent matrix grains contribute to the amplitude of driving forces for AGG, which makes Goss grains break through the pinning and grow abnormally during the whole heating process. Therefore, the secondary recrystallization in binary Fe₈₁Ga₁₉ alloy is realized in terms of the controllable grain boundary mobility difference between Goss and matrix grains. This viewpoint can be generalized to Fe-Ga alloy and the other BCC alloy with a similarity of grain boundary characteristic, and can stimulate novel potential energy-efficient production technology for secondary recrystallization.

5. Conclusions

1. The rolled binary Fe₈₁Ga₁₉ sheets with accurately centimeter-sized Goss grains were successfully produced by the inherent grain boundary mobility difference between Goss and matrix grains without conventional dependence on inhibitor and surface energy effects.
2. A special, fine-grained primarily-recrystallized texture consisting of strong {112}–{111}<110> texture and weak Goss texture provides the inherent pinning effect for normal grain growth by a large fraction of low angle grain boundaries ($< 15^\circ$) and very high angle grain boundaries ($> 45^\circ$). More high energy grain boundaries ($20\text{--}45^\circ$) around Goss grains supplies an advantage in grain boundary mobility for the preferential growth of Goss grains.
3. Based on the development of grain orientation and grain boundary character distribution from 950 °C to 1025 °C by quasi-situ electron backscatter diffraction, the AGG of Goss grains originates from the preferred grain boundary mobility by the much higher fraction of the HEGBs around

Goss grains, coupled with the orientation and misorientation angle distribution of adjacent matrix grains. The present result suggests that the complete secondary recrystallization can be realized by the inherent grain boundary mobility difference between target orientation and matrix grains in Fe-based, and other BCC alloys.

Author Contributions: Conceptualization, Y.S. and L.Z.; software, Z.H. and N.S.; validation, Z.H., Y.G., and F.Z.; formal analysis, Z.H. and F.L.; investigation, Z.H. and Y.S.; resources, Y.S.; data curation, Z.H.; writing—original draft preparation, Z.H.; writing—review and editing, Z.H. and Y.H.; visualization, N.S.; supervision, Y.S. and L.Z.; project administration, Y.H. and F.Z.; funding acquisition, Y.S.

Funding: This research was funded by the National Key R&D Program of China, grant number 2016YFB0300305; the National Natural Science Foundation of China, grant number 51671049; the Chinese Postdoctoral Science Foundation, grant number 2018M640257; the Inner Mongolia Natural Science Foundation, grant number 2018ZD10; and the Key Laboratory Open Fund of Baiyunobo Rare Earth Resource Researches and Comprehensive Utilization, grant number 2017Z1953.

Conflicts of Interest: The authors declare no conflict of interest.

References

- Clark, A.E.; Restorff, J.B.; Wun-Fogle, M.; Lograsso, T.A.; Schlagel, D.L. Magnetostrictive properties of body-centered cubic Fe-Ga and Fe-Ga-Al alloys. *IEEE Trans. Magn.* **2000**, *36*, 3238–3240. [[CrossRef](#)]
- Guruswamy, S.; Srisukhumbowornchai, N.; Clark, A.E.; Restorff, J.B.; Wun-Fogle, M. Strong, ductile, and low-field-magnetostrictive alloys based on Fe-Ga. *Scr. Mater.* **2000**, *43*, 239–244. [[CrossRef](#)]
- Kellogg, R.A.; Russell, A.M.; Lograsso, T.A.; Flatau, A.B.; Clark, A.E.; Wun-Fogle, M. Tensile properties of magnetostrictive iron-gallium alloys. *Acta Mater.* **2004**, *52*, 5043–5050. [[CrossRef](#)]
- Srisukhumbowornchai, N.; Guruswamy, S. Large magnetostriction in directionally solidified FeGa and FeGaAl alloys. *J. Appl. Phys.* **2001**, *90*, 5680–5688. [[CrossRef](#)]
- Kellogg, R.A.; Flatau, A.B.; Clark, A.E.; Wun-Fogle, M.; Lograsso, T.A. Texture and grain morphology dependencies of saturation magnetostriction in rolled polycrystalline Fe₈₃Ga₁₇. *J. Appl. Phys.* **2003**, *93*, 8495–8497. [[CrossRef](#)]
- Na, S.M.; Flatau, A.B. Secondary recrystallization, crystallographic texture and magnetostriction in rolled Fe-Ga based alloys. *J. Appl. Phys.* **2007**, *101*, 09N518. [[CrossRef](#)]
- Na, S.M.; Yoo, J.H.; Flatau, A.B. Abnormal (110) grain growth and magnetostriction in recrystallized galphenol with dispersed niobium carbide. *IEEE Trans. Magn.* **2009**, *45*, 4132–4135.
- He, Z.H.; Sha, Y.H.; Fu, Q.; Lei, F.; Jin, B.K.; Zhang, F.; Zuo, L. Sharp Goss texture and magnetostriction in binary Fe₈₁Ga₁₉ sheets. *J. Magn. Magn. Mater.* **2016**, *417*, 321–326. [[CrossRef](#)]
- Fu, Q.; Sha, Y.H.; He, Z.H.; Lei, F.; Zhang, F.; Zuo, L. Recrystallization texture and magnetostriction in binary Fe₈₁Ga₁₉ sheets. *Acta Metall. Sin.* **2017**, *53*, 90–96.
- Matsuo, M. Texture control in the production of grain oriented silicon steels. *ISIJ Int.* **1989**, *29*, 809–827. [[CrossRef](#)]
- Morawiec, A. Grain misorientations in theories of abnormal grain growth in silicon steel. *Scr. Mater.* **2000**, *43*, 275–278. [[CrossRef](#)]
- Hayakawa, Y.; Muraki, M.; Szpunar, J.A. The changes of grain boundary character distribution during the secondary recrystallization of electrical steel. *Acta Mater.* **1998**, *46*, 1063–1073. [[CrossRef](#)]
- Lin, P.; Palumbo, G.; Harase, J.; Aust, K.T. Coincidence Site Lattice (CSL) grain boundaries and Goss texture development in Fe-3% Si alloy. *Acta Mater.* **1996**, *44*, 4677–4683. [[CrossRef](#)]
- Rajmohan, N.; Szpunar, J.A.; Hayakawa, Y. A role of fractions of mobile grain boundaries in secondary recrystallization of Fe-Si steels. *Acta Mater.* **1999**, *47*, 2999–3008. [[CrossRef](#)]
- Heo, N.H.; Chai, K.H.; Na, J.G. Correlation between interfacial segregation and surface-energy-induced selective grain growth in 3% silicon-iron alloy. *Acta Mater.* **2000**, *48*, 2901–2910. [[CrossRef](#)]
- Na, S.M.; Flatau, A.B. Single grain growth and large magnetostriction in secondarily recrystallized Fe-Ga thin sheet with sharp Goss (011)[100] orientation. *Scr. Mater.* **2012**, *66*, 307–310. [[CrossRef](#)]
- Na, S.M.; Atwater, K.M.; Flatau, A.B. Particle pinning force thresholds for promoting abnormal grain growth in magnetostrictive Fe-Ga alloy sheets. *Scr. Mater.* **2015**, *100*, 1–4. [[CrossRef](#)]

18. Yuan, C.; Li, J.H.; Zhang, W.L.; Bao, X.G.; Gao, X.X. Sharp Goss orientation and large magnetostriction in the rolled columnar-grained Fe-Ga alloys. *J. Magn. Magn. Mater.* **2015**, *374*, 459–462. [[CrossRef](#)]
19. Li, J.H.; Yuan, C.; Qi, Q.L.; Bao, X.Q.; Gao, X.X. Effect of initial oriented columnar grains on the texture evolution and magnetostriction in Fe-Ga rolled sheets. *Metals* **2017**, *7*, 36. [[CrossRef](#)]
20. Liu, Y.Y.; Li, J.H.; Gao, X.X. Influence of intermediate annealing on abnormal Goss grain growth in the rolled columnar-grained Fe-Ga-Al alloys. *J. Magn. Magn. Mater.* **2017**, *435*, 194–200. [[CrossRef](#)]
21. He, Z.H.; Hao, H.B.; Sha, Y.H.; Li, W.L.; Zhang, F.; Zuo, L. Sharp secondary recrystallization and large magnetostriction in Fe₈₁Ga₁₉ sheet induced by composite nanometer-sized inhibitors. *J. Magn. Magn. Mater.* **2019**, *478*, 109–115. [[CrossRef](#)]
22. Summers, E.M.; Meloy, R.; Na, S.M. Magnetostriction and texture relationships in annealed galfenol alloys. *J. Appl. Phys.* **2009**, *105*, 07A922. [[CrossRef](#)]
23. He, Z.H.; Sha, Y.H.; Fu, Q.; Lei, F.; Zhang, F.; Zuo, L. Secondary recrystallization and magnetostriction in binary Fe₈₁Ga₁₉ thin sheets. *J. Appl. Phys.* **2016**, *119*, 123904. [[CrossRef](#)]
24. Kestens, L.; Jonas, J.J.; Van Houtte, P.; Aernoudt, E. Orientation selective recrystallization of nonoriented electrical steels. *Metall. Mater. Trans. A* **1996**, *27*, 2347–2358. [[CrossRef](#)]
25. He, Z.H.; Sha, Y.H.; Zhang, F.; Lin, F.F.; Zuo, L. Development of Strong η Fiber Recrystallization Texture in Rolled Fe₈₁Ga₁₉ Thin Sheet. *Metall. Mater. Trans. A* **2014**, *45A*, 129–133. [[CrossRef](#)]
26. Samajdar, I.; Cicale, S.; Verlinden, B.; Van Houtte, P.; Abbruzzese, G. Primary recrystallization in a grain oriented silicon steel: On the origin of Goss{110}[001] grains. *Scr. Mater.* **1998**, *39*, 1083–1088. [[CrossRef](#)]
27. Park, J.T.; Szipunar, J.A. Evolution of recrystallization texture in nonoriented electrical steels. *Acta Mater.* **2003**, *51*, 3037–3051. [[CrossRef](#)]
28. Cheng, Z.Y.; Liu, J.; Zhu, J.C.; Xiang, Z.D.; Jia, J.; Bi, Y.J. Microstructure, texture evolution and magnetic properties of Fe-6.5 wt. % Si and Fe-6.5 wt. % Si-0.5 wt. % Cu alloys during rolling and annealing treatment. *Metals* **2018**, *8*, 144. [[CrossRef](#)]
29. Liu, J.L.; Sha, Y.H.; Zhang, F.; Li, J.C.; Yao, Y.C.; Zuo, L. Development of {210}<001> recrystallization texture in Fe-6.5 wt. % Si thin sheets. *Scr. Mater.* **2011**, *65*, 292–295. [[CrossRef](#)]
30. Fu, Q.; Sha, Y.H.; Zhang, F.; Esling, C.; Zuo, L. Correlative effect of critical parameters for η recrystallization texture development in rolled Fe₈₁Ga₁₉ sheet: Modeling and experiment. *Acta Mater.* **2019**, *167*, 167–180. [[CrossRef](#)]
31. He, Y.; Coey, J.M.D.; Schaefer, R.; Jiang, C. Determination of bulk domain structure and magnetization processes in bcc ferromagnetic alloys: Analysis of magnetostriction in Fe₈₃Ga₁₇. *Phys. Rev. Mater.* **2018**, *2*, 014412. [[CrossRef](#)]
32. Omura, T.; Hayakawa, Y. Influence of Primary-Recrystallization Texture on Selective Growth of Goss Grains. *Mater. Trans.* **2013**, *54*, 14–21. [[CrossRef](#)]
33. Hayakawa, Y.; Omura, T.; Imamura, T. Onset of Secondary Recrystallization in High Purity 3.3% Si Steel. *ISIJ Int.* **2014**, *54*, 2385–2393. [[CrossRef](#)]
34. Chen, N.; Zaefferer, S.; Lahn, L.; Günther, K.; Raabe, D. Effects of topology on abnormal grain growth in silicon steel. *Acta Mater.* **2003**, *51*, 1755–1765. [[CrossRef](#)]
35. Morawiec, A. On abnormal growth of Goss grains in grain-oriented silicon steel. *Scr. Mater.* **2011**, *64*, 466–469. [[CrossRef](#)]
36. Homma, H.; Hutchinson, B.; Kubota, T. The production mechanism of extensively sharp Goss orientation in HI-B material. *J. Magn. Magn. Mater.* **2003**, *254*, 331–333. [[CrossRef](#)]
37. Ono, N.; Kimura, K.; Watanabe, T. Monte Carlo simulation of grain growth with the full spectra of grain orientation and grain boundary energy. *Acta Mater.* **1999**, *47*, 1007–1017. [[CrossRef](#)]
38. Rajmohan, N.; Szipunar, J.A. An analytical method for characterizing grain boundaries around growing Goss grains during secondary recrystallization. *Scr. Mater.* **2001**, *44*, 2387–2392. [[CrossRef](#)]

